Since January 2020 Elsevier has created a COVID-19 resource centre with free information in English and Mandarin on the novel coronavirus COVID-19. The COVID-19 resource centre is hosted on Elsevier Connect, the company's public news and information website.

Virology **272,** 27–39 (2000)
doi:10.1006/viro.2000.0330, available online at http://www.idealibrary.com on IDEAL®

Further Characterization of the Coronavirus Infectious Bronchitis Virus 3C-like Proteinase and Determination of a New Cleavage Site

Lisa F. P. Ng and D. X. Liu[1]

Institute of Molecular Agrobiology, The National University of Singapore, 1 Research Link, Singapore 117604

Received December 10, 1999; returned to author for revision March 14, 2000; accepted March 29, 2000

Coronavirus infectious bronchitis virus (IBV) encodes a trypsin-like proteinase (3C-like proteinase) by ORF 1a, which has been demonstrated to play a pivotal role in proteolytic processing of gene 1-encoded polyproteins. In our previous studies, the proteinase was identified as a 33-kDa protein in IBV-infected cells, and its catalytic center was shown to consist of H^{2820} and C^{2922} residues. It is released from the 1a and 1a/1b polyproteins by autoprocessing at two Q–S dipeptide bonds (Q^{2779}–S^{2780} and Q^{3086}–S^{3087}). In this report, further characterization of the two cleavage sites demonstrates that the N-terminal Q^{2779}–S^{2780} site is tolerant to mutations at the P1 position. Deletion of the C-terminal region of the proteinase shows that a significant amount of the enzymatic activity is maintained upon deletion of up to 67 amino acids, suggesting that the extreme C-terminal region may be dispensable for the proteolytic activity of the proteinase. Analysis of the autoprocessing kinetics *in vitro* reveals that proteolysis at the Q^{2779}–S^{2780} site is the first cleavage event mediated by this proteinase. This is followed by cleavage at the Q^{3086}–S^{3087} site. The occurrence of both cleavage events in intact cells is potentially rapid and efficient, as no intermediate cleavage products covering the proteinase were detected in either IBV-infected or transfected cells. Immunofluorescence microscopy and subcellular fractionation studies further show differential subcellular localization of the proteinase in IBV-infected cells and in cells expressing the 3C-like proteinase alone, indicating that additional roles in viral replication might be played by this protein. Finally, a Q–A (Q^{3379}–A^{3380}) dipeptide bond encoded by nucleotides 10,663 to 10,668 was demonstrated to be a cleavage site of the proteinase.

INTRODUCTION

The avian coronavirus infectious bronchitis virus (IBV) is now categorized under a new order, Nidovirales (Cavanagh, 1997; de Vries *et al.,* 1997). Its 27.6-kb genome-length mRNA, mRNA1, is composed of two large overlapping ORFs (1a and 1b) at the 5′-unique region and encodes a fusion polyprotein of 741 kDa by a unique frameshifting mechanism (Boursnell *et al.,* 1987; Brierly *et al.,* 1987, 1989). Proteolytic processing of the 441-kDa 1a and 741-kDa 1a/1b fusion polyproteins to smaller mature products is mediated by viral proteinases. Three proteinase domains, namely, two overlapping papain-like proteinase domains and a picornavirus 3C-like proteinase domain (3C-like proteinase) (Fig. 1a), have been predicted to be encoded by ORF 1a (Boursnell *et al.,* 1987; Gorbalenya *et al.,* 1989; Lee *et al.,* 1991).

In recent years, progress has been made in the identification and characterization of the proteinase activities as well as their cleavage products. The first papain-like proteinase domain is involved in proteolytic cleavage of the N-terminal region of the 1a and 1a/1ab polyproteins to release an 87-kDa protein and a 195-kDa protein and the N-terminus of a 41-kDa product in IBV-infected cells (Liu *et al.,* 1995; Lim and Liu, 1998; Lim *et al.,* 2000). Similar enzymatic activities were also reported for the first papain-like proteinase domain of human and murine coronaviruses. In mouse hepatitis virus (MHV), two N-terminal cleavage products (p28 and p65) have been reported (Hughes *et al.,* 1995; Bonilla *et al.,* 1997; Baker *et al.,* 1989, 1993; Dong and Baker, 1994; Gao *et al.,* 1996; Schiller *et al.,* 1998). The same domain of human coronavirus (HCV) processes the two polyproteins to release p9 (Herold *et al.,* 1998).

Important roles in processing of the 1a and 1a/1b polyproteins are also played by the 3C-like proteinase domain. Characterization of the proteinase activities has shown that it cleaves the bulk of the polyproteins at conserved Q–S (G and N) dipeptide bonds, resulting in the release of more than 10 mature products (Liu *et al.,* 1994, 1995, 1997, 1998; Ng and Liu, 1998; Tibbles *et al.,* 1999; Ziebuhr and Siddell, 1999; Grotzinger *et al.,* 1996; Heusipp *et al.,* 1997a, b; Lu *et al.,* 1995, 1998; Schiller *et al.,* 1998). The proteinase was identified as a 27-kDa protein for MHV (Lu *et al.,* 1996) and a 34-kDa protein for HCV (Ziebuhr *et al.,* 1995). The catalytic center of the proteinase consists of a His residue and a Cys residue (Liu and Brown, 1995; Lu *et al.,* 1995; Seybert *et al.,* 1997; Ziebuhr *et al.,* 1995, 1997).

The 3C-like proteinase domain is flanked by hydrophobic regions in the coronaviral genomes. *In vitro* studies in

[1] To whom correspondence and reprint requests should be addressed. E-mail: liudx@ima.org.sg.

0042-6822/00 $35.00

MHV have shown that its enzymatic activity can be greatly enhanced by the addition of canine pancreatic microsomal membranes to the translation reaction mixture (Pinon *et al.,* 1997; Schiller *et al.,* 1998). The proteolytic activity of the proteinase could be inhibited by a variety of cysteine and serine inhibitors and was eliminated by the cysteine proteinase inhibitor E64d (Lu *et al.,* 1996; Pinon *et al.,* 1997; Seybert *et al.,* 1997). More recently, immunofluorescence studies using region-specific antisera against several 1a and 1a/1b cleavage products including the 3C-like proteinase have suggested that the proteinase may be associated with the viral RNA replication–transcription machinery (Schiller *et al.,* 1998; Ziebuhr and Siddell, 1999; Shi *et al.,* 1999; Denison *et al.,* 1999; van der Meer *et al.,* 1999).

In a previous study, we identified the IBV 3C-like proteinase as a 33-kDa protein in IBV-infected Vero cells (Lim *et al.,* 2000). The proteinase was shown to be self-cleaved from the polyproteins at the two previously predicted Q–S dipeptide bonds (Q^{2779}–S^{2780} and Q^{3086}–S^{3087}) in an *in vitro* processing assay (Tibbles *et al.,* 1996). The *in vitro* proteolytic activity was shown to be strictly dependent on the addition of canine microsomal membranes (Tibbles *et al.,* 1996). Here, we show, by deletion and mutational analyses, that the N-terminal cleavage site of the 3C-like proteinase is tolerant to mutations and the extreme C-terminal region may be dispensable for the enzymatic activity. The proteinase could be self-cleaved to the 33-kDa mature form *in vitro* in rabbit reticulocyte lysate without the addition of canine microsomal membranes. Immunofluorescence staining and cellular fractionation studies demonstrated that the proteinase is associated mainly with the membrane fraction in virus-infected cells. However, a free distribution pattern was observed when the proteinase was overexpressed in intact cells. Finally, instead of the previously predicted Q^{3365}–G^{3366} dipeptide bond, the Q^{3379}–A^{3380} dipeptide bond was identified as a cleavage site of the proteinase.

RESULTS

Tolerance of the N-terminal cleavage site (Q^{2779}–S^{2780}) of the 3C-like proteinase to mutations

The previously predicted Q^{2779}–S^{2780} dipeptide bond was shown to be the N-terminal cleavage site of the 3C-like proteinase in an *in vitro* processing assay (Tibbles *et al.,* 1996). Substitution mutagenesis was carried out to investigate the effects of mutations on the self-cleavage efficiency of the proteinase at this position. The Q^{2779}–S^{2780} dipeptide bond was first mutated to E^{2779}–S^{2780}, giving rise to pIBV9Δ1Q^{2779}–E (Fig. 1a). Expression of pIBV9Δ1Q^{2779}–E led to the detection of three protein species (Fig. 1b, lane 2). In addition to the 33-kDa protein, two products of approximately 43 and 48 kDa, respectively, were also detected (Fig. 1b, lane 2). The 43-kDa protein may represent a fusion product containing the 33-kDa protein and the product encoded by nucleotides 8693 to 8865, and the 48-kDa protein may represent the full-length product encoded by this construct (Fig. 1a). As a significant amount of the 33-kDa protein was detected from the expression of this construct (Fig. 1b, lane 2), this result indicates that an E–S dipeptide could be used efficiently by the 3C-like proteinase at this position. Substitution of the Q^{2779} residue with a K was then carried out, giving rise to pIBV9Δ1Q^{2779}–K (Fig. 1a). Expression of this construct resulted in more efficient detection of the 43- and 48-kDa products (Fig. 1b, lane 3). However, a trace amount of the 33-kDa protein was still detected (Fig. 1b, lane 3). These results suggest that cleavage at the Q^{2779}–S^{2780} dipeptide bond may be tolerant to mutations and the Q to E substitution is better tolerated than the Q–K substitution.

Mutation and deletion analyses of the C-terminal region of the 3C-like proteinase

Mutation of the C-terminal cleavage site (Q^{3086}–S^{3087} dipeptide bond) of the 3C-like proteinase to E^{3086}–S^{3087} was subsequently made, giving rise to pIBV9Q^{3086}–E (Fig. 2a). Expression of pIBV9Q^{3086}–E led to the detection of a novel product with an apparent molecular mass of approximately 35 kDa (Fig. 2b, lane 2). No 33-kDa protein was observed (Fig. 2b, lane 2). This was unexpected, as no further cleavage site was predicted to be located 30–60 bp downstream of the Q^{3086}–S^{3087} dipeptide bond. To investigate the possibility that the C-terminus of the 35-kDa protein may be derived from a novel cleavage site located 10 to 20 amino acid residues downstream of the Q^{3086} residue, two deletion plasmids, pIBV9Q^{3086}–EΔ1 and pIBV9Q^{3086}–EΔ2, were constructed. As can be seen in Fig. 2a, the IBV sequence present in pIBV9Q^{3086}–EΔ1

FIG. 1. (a) Diagram of ORF1a, illustrating the two overlapping papain-like proteinase domains (PLPDs) and the 3C-like proteinase domain (3CLP). The Q^{2779}–S^{2780}, Q^{3086}–S^{3087}, Q^{3379}–A^{3380}, and Q^{3462}–S^{3463} scissile bonds and viral products generated from cleavage by the 3C-like proteinase are indicated. Also shown are the IBV sequence recognized by anti-3C, the stretches of hydrophobic residues encoded by ORF1a and the IBV sequences present in pIBV9, pIBV9Δ1Q^{2779}–E, and pIBV9Δ1Q^{2779}–K. The viral products generated from cleavage by the 3C-like proteinase and the full-length products encoded by some plasmids are illustrated. The molecular masses of these products were estimated according to their migration on SDS–PAGE. The Q^{2779}–S^{2780}, Q^{3086}–S^{3087}, Q^{3379}–A^{3380}, and Q^{3462}–S^{3463} residues are encoded by nucleotides 8863–8868, 9784–9789, 10,663–10,668, and 10,912–10,917, respectively. (b) Mutational analysis of the Q^{2779}–S^{2780} dipeptide bond. Plasmids pIBV9, pIBV9Δ1Q^{2779}–E, and pIBV9Δ1Q^{2779}–K, respectively, were transiently expressed in Cos-7 cells using the vaccinia-T7 expression system. Cells were labeled with [^{35}S]methionine–cysteine, lysates were prepared, and polypeptides were immunoprecipitated with anti-3C. Gel electrophoresis of the polypeptides was performed on an SDS–12.5% polyacrylamide gel and polypeptides were detected by fluorography.

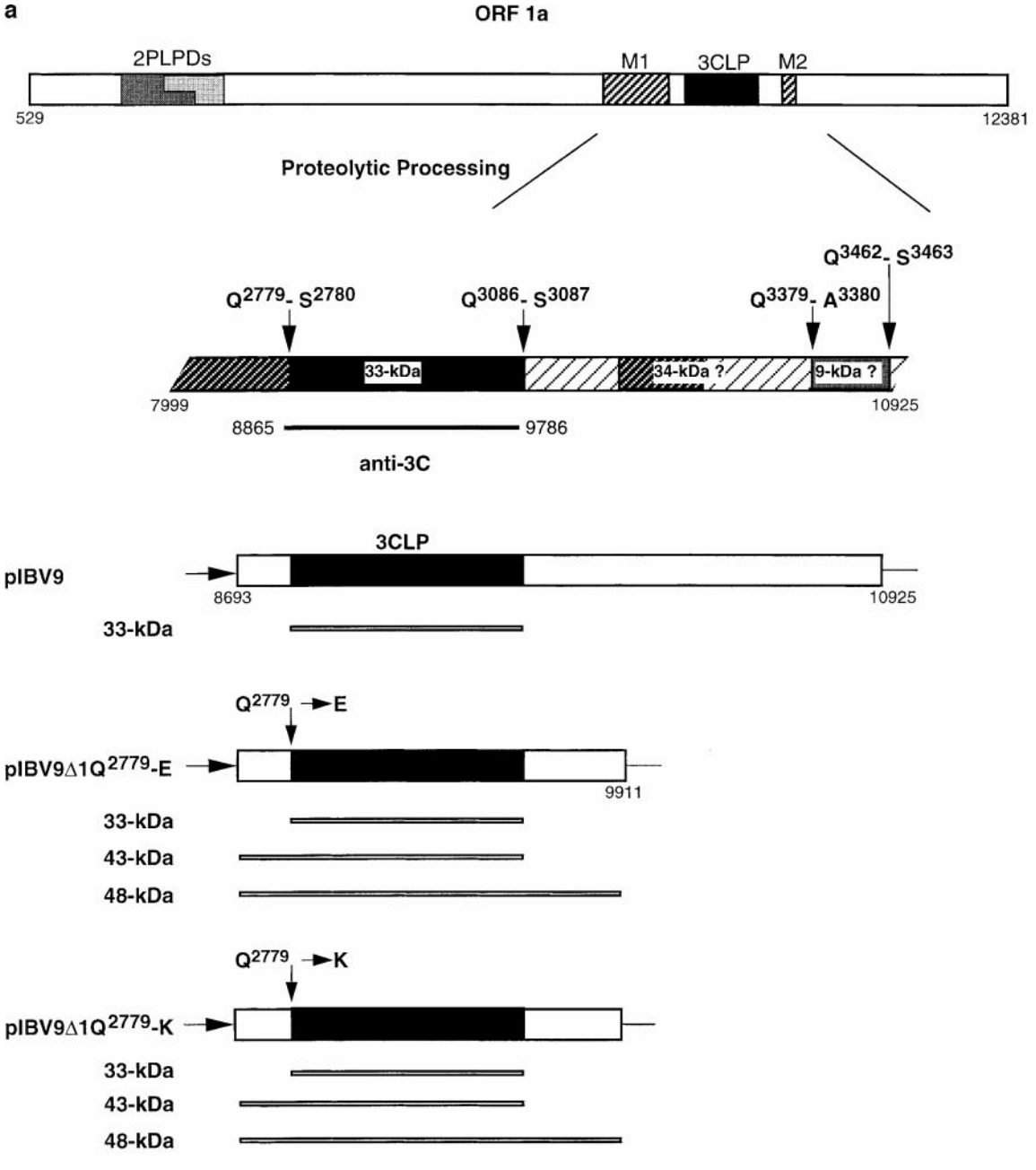
a
ORF 1a
2PLPDs
M1
3CLP
M2
529
12381
Proteolytic Processing
Q2779- S2780
Q3086- S3087
Q3379- A3380
Q3462- S3463
33-kDa
34-kDa ?
9-kDa ?
7999
10925
8865
9786
anti-3C
3CLP
pIBV9
8693
10925
33-kDa
Q2779 →E
pIBV9Δ1Q2779-E
9911
33-kDa
43-kDa
48-kDa
Q2779 →K
pIBV9Δ1Q2779-K
33-kDa
43-kDa
48-kDa
b
pIBV9
pIBV9Δ1Q2779-E
pIBV9Δ1Q2779-K
69
46
30
48 kDa
43 kDa
33 kDa
1
2
3

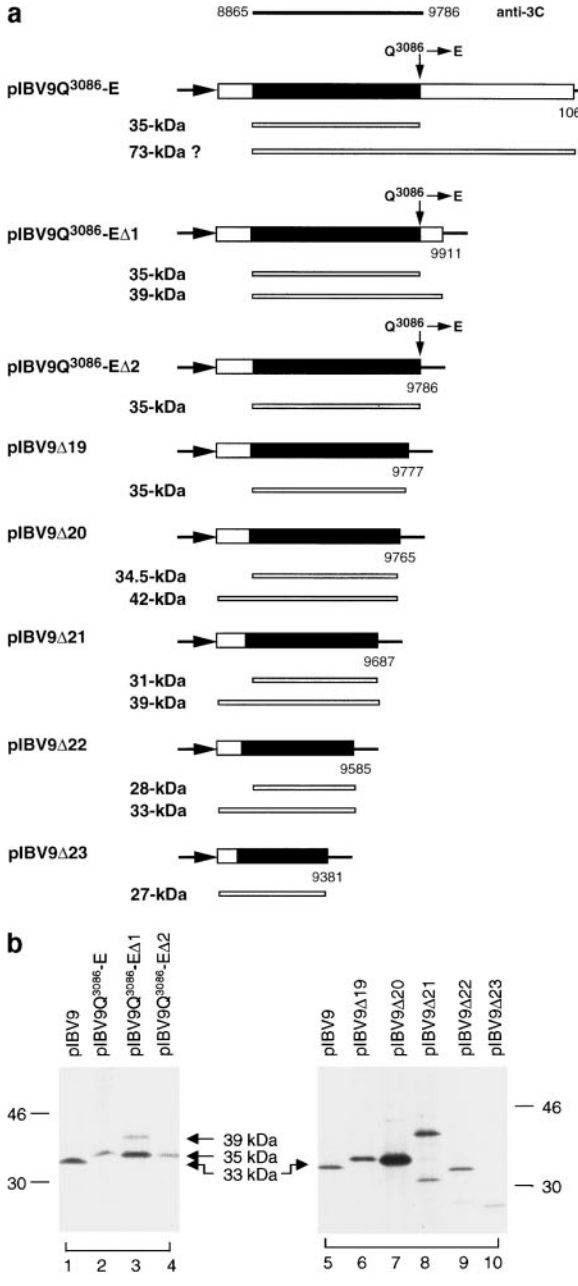

FIG. 2. (a) Diagram showing the IBV sequences present in pIBV9Q^{3086}–E, pIBV9Q^{3086}–EΔ1, pIBV9Q^{3086}–EΔ2, pIBV9Δ19, pIBV9Δ20, pIBV9Δ21, pIBV9Δ22, and pIBV9Δ23. The viral products generated from cleavage by the 3C-like proteinase and the full-length products encoded by some plasmids are illustrated. The molecular masses of these products were estimated according to their migration on SDS–PAGE. The Q^{3086} residue is encoded by nucleotides 9784–9786. (b) Mutational and deletion analyses of the Q^{3086}–S^{3087} dipeptide bond and the C-terminal region of the 3C-like proteinase. Plasmids pIBV9, pIBV9Q^{3086}–E, pIBV9Q^{3086}–EΔ1, pIBV9Q^{3086}–EΔ2, pIBV9Δ19, pIBV9Δ20, pIBV9Δ21, pIBV9Δ22, and pIBV9Δ23, respectively, were transiently expressed in Cos-7 cells using the vaccinia-T7 system. The cells were labeled with [^{35}S]methionine–cysteine, lysates were prepared, and the labeled polypeptides were immunoprecipitated with anti-3C. Gel electrophoresis of the polypeptides was performed on an SDS–12.5% polyacrylamide gel and polypeptides were detected by fluorography.

was terminated at nucleotide position 9911. Expression of this construct, once again, led to the detection of the 35-kDa protein (Fig. 2b, lane 3). Meanwhile, a novel product migrating more slowly than the 35-kDa protein was also detected (Fig. 2b, lane 3). Its apparent molecular mass of 39 kDa suggests that it is a fusion product containing the 35-kDa protein and the product encoded by nucleotides up to 9911. pIBV9Q^{3086}–EΔ2 was constructed by introducing a UGA termination codon immediately downstream of the Q^{3086} residue (Fig. 2a). Interestingly, expression of this plasmid led to the detection of a single protein species comigrating with the 35-kDa protein processed from pIBV9Q^{3086}–EΔ1 (Fig. 2b, lane 4), suggesting that the E^{3086} residue is actually the C-terminus of the 35-kDa protein expressed from pIBV9Q^{3086}–E and pIBV9Q^{3086}–EΔ1. These results demonstrate that mutation of the Q^{3086} residue to an E only marginally reduces the cleavage efficiency occurring at the Q^{3086}–S^{3087} dipeptide bond, but alters the mobility of the 33-kDa protein on SDS–PAGE.

To investigate the possibility that the C-terminal region of the 3C-like proteinase may contain sequences nonessential for the catalytic activity of the proteinase, five deletion constructs, pIBV9Δ19, pIBV9Δ20, pIBV9Δ21, pIBV9Δ22, and pIBV9Δ23, were made and expressed in intact cells. These constructs encode proteins with deletions of 3, 7, 33, 67, and 135 amino acid residues, respectively, from the C-terminus of the 3C-like proteinase. Expression of pIBV9Δ19 and pIBV9Δ20 showed that almost full enzymatic activity was maintained upon the deletions. As can be seen, a 35-kDa product representing the C-terminally truncated form of the 3C-like proteinase was detected in both cases (Fig. 2b, lanes 6 and 7). No full-length product was observed from the expression of pIBV9Δ19 (Fig. 2b, lane 6), but a trace amount of the full-length product was detected from the expression of pIBV9Δ20 (Fig. 2b, lane 7). Progressively less enzymatic activity was observed when pIBV9Δ21 and pIBV9Δ22 were expressed. In each case, two products representing the full-length proteins and the C-terminally truncated 3C-like proteinase were detected (Fig. 2b, lanes 8 and 9). Expression of pIBV9Δ23 showed the detection of the full-length product only (Fig. 2b, lane 10), indicating that the catalytic activity was abolished by this deletion. These results suggest that the extreme C-terminal region is not essential for the catalytic activity of the 3C-like proteinase.

Characterization of the *in vitro* enzymatic activity of the 3C-like proteinase

Studies on the 3C-like proteinase of human and murine coronaviruses have demonstrated that microsomal membranes are not strictly required for the *in vitro* cleavage activity but addition of the membranes can greatly enhance the autoprocessing activity of the proteinase

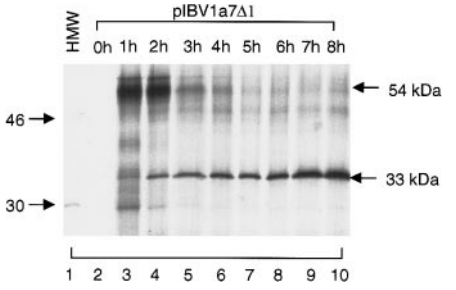

FIG. 3. Time course analysis of the autoprocessing of the 3C-like proteinase expressed from pIBV1a7Δ1 in rabbit reticulocyte lysates. A 10-fold excess of unlabeled methionine was added to the *in vitro* translation reaction after incubation at 30°C for 10 min. Aliquots were subsequently taken from the reaction after incubation for 0, 1, 2, 3, 4, 5, 6, 7, and 8 h. The [^{35}S]methionine-labeled products were separated on an SDS–12.5% polyacrylamide gel and detected by fluorography.

(Lu *et al.,* 1996; Pinon *et al.,* 1997; Schiller *et al.,* 1998; Heusipp *et al.,* 1997a). However, the microsomal membranes were shown to be indispensable for the *in vitro* activity of the IBV 3C-like proteinase (Tibbles *et al.,* 1996). To clarify this discrepancy, plasmid pIBV1a7Δ1, which covers nucleotides 7999 to 9786 and contains the upstream hydrophobic region (M1), was expressed *in vitro* in a rabbit reticulocyte lysate system and pulse–chased for up to 8 h. Aliquots were removed at the indicated time and the reactions were stopped by the addition of RNase A. The 33-kDa protein was detected after incubation for 1 h and its expression steadily increased toward the end of the time course (Fig. 3). The expression of the full-length 54-kDa protein meanwhile decreased rapidly over time (Fig. 3). The addition of microsomal membranes did not significantly increase the autoprocessing rate of the 33-kDa protein (data not shown). These results demonstrate that autoprocessing of the IBV 3C-like proteinase could occur *in vitro* in reticulocyte lysate in the absence of the membranes.

In vitro autoprocessing kinetics of the 3C-like proteinase

The *in vitro* processing system was then used to study the autoprocessing kinetics of the IBV 3C-like proteinase. Plasmids pIBV9Q^{3086}–EΔ1 and its parental construct pIBV1a9Δ17 (Fig. 4a) were expressed in reticulocyte lysate and pulse–chased for up to 2 h. The full-length 48-kDa product was observed from the expression of both constructs after chase for 10 min, and its expression gradually decreased toward the end of the time course (Fig. 4b). The appearance of a 39-kDa product, representing the fusion protein containing the 3C-like proteinase and the product encoded by nucleotides 9787 to 9910, was observed after chase for 20 min (Fig. 4b). It peaks after chase for 60 min and then starts to decline (Fig. 4b). The 33-kDa protein was first seen from the expression of pIBV1a9Δ17 after chase for 30 min and gradually increased toward the end of the time course (Fig. 4b). The 35-kDa mutant 3C-like proteinase expressed from pIBV9Q^{3086}–EΔ1 appeared slightly later than the wild-type proteinase. It was first seen after chase for 40 min (Fig. 4b, lane 14).

Differential subcellular localization of the 3C-like proteinase in virus-infected and transfected cells

Determination of the subcellular localization of ORF 1a-encoded viral products from the Nidovirales family, namely, MHV-A59, MHV-JHM, HCV-229E, and equine arteritis virus (EAV), was the subject of several recent reports (Shi *et al.,* 1999; Schiller *et al.,* 1998; Ziebuhr and Siddell, 1999; van der Meer *et al.,* 1998, 1999). It was interesting to note that immunofluorescence staining of viral infected cells using anti-3C antiserum showed distinct punctuate perinuclear staining patterns (Schiller *et al.,* 1998; Shi *et al.,* 1999; Denison *et al.,* 1999; van der Meer *et al.,* 1999), suggesting that the proteinase may be associated with intracellular membranes. To study the subcellular localization patterns of the IBV 3C-like proteinase, the proteinase was tagged to an 11-amino-acid T7 tag (MASMTGGQQMG) derived from the major capsid protein of bacteriophage T7, and a highly specific anti-T7 monoclonal antibody (Novagen) was used to stain cells overexpressing the fusion protein. This procedure is used to avoid the high background of the anti-3C polyclonal antiserum when it was used in indirect immunofluorescence assays. As can be seen in Figs. 5A and 5B, staining of Vero cells expressing the T7 tagged 3C-like proteinase with anti-T7 antibody showed a diffuse cytoplasmic staining profile. Indirect immunofluorescence staining of IBV-infected Vero cells with anti-3C antiserum showed a distinct perinuclear punctate pattern at 13 h postinfection (Fig. 5D), although high background was also observed for the mock-infected cells (Fig. 5C). This distribution pattern is similar to those reported for other coronaviruses and arteriviruses (Schiller *et al.,* 1998; Shi *et al.,* 1999; van der Meer *et al.,* 1998). These results suggest that the IBV 3C-like proteinase may exhibit differential subcellular distribution patterns in virus-infected cells and in transfected cells. When it was expressed individually, a diffuse distribution profile was observed. However, the proteinase was shown to be associated with intracellular membranous structures in virus-infected cells.

Subcellular fractionation of pIBV3C-transfected and IBV-infected cells was then carried out to investigate this possibility further. Two fractions, namely, the membrane and cytosol fractions, were collected and subjected to immunoprecipitation with anti-3C antiserum. Figure 6a shows that approximately equal amounts of the 33-kDa proteinase were detected from both fractions (Fig. 6a, lanes 1 and 3). Quantification by densitometry confirmed that the membrane and cytosol fractions contain 50.19

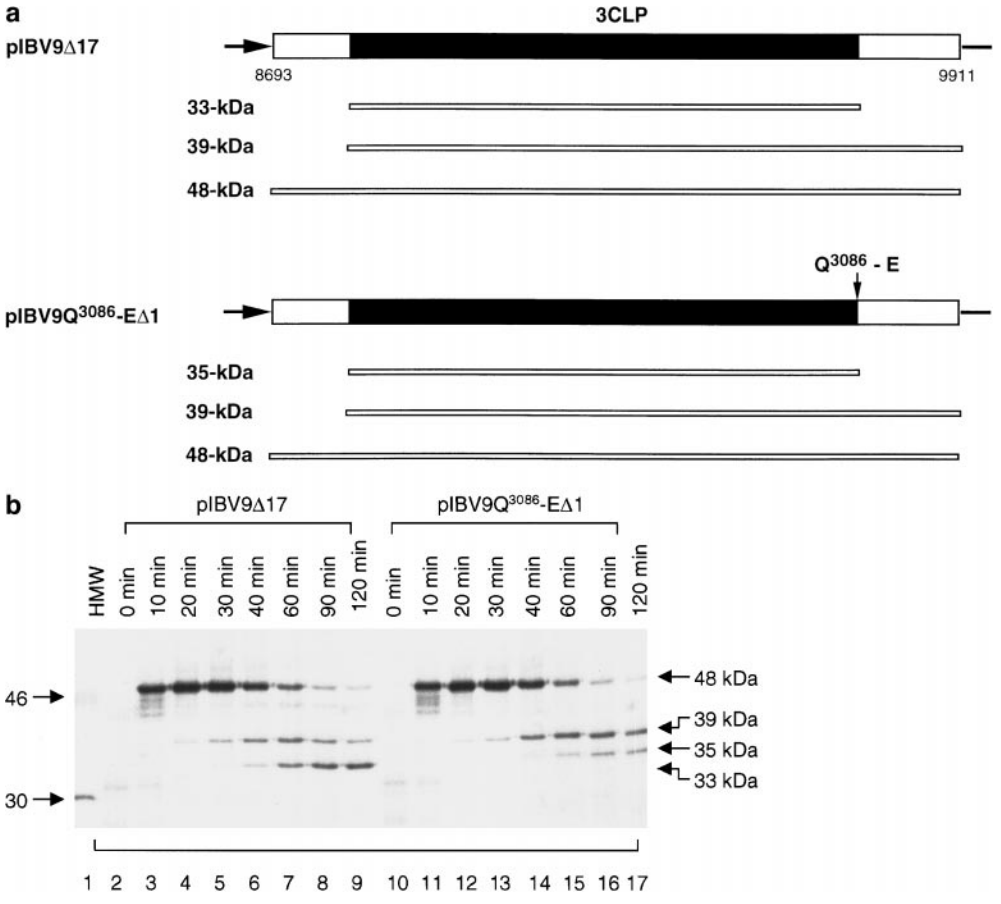

FIG. 4. (a) Diagram showing the IBV sequences present in pIBV9Δ17 and pIBV9Q^{3086}–EΔ1. The viral products generated from cleavage by the 3C-like proteinase and the full-length products encoded by the two plasmids are illustrated. The molecular masses of these products were estimated according to their migration on SDS–PAGE. The Q^{3086} residue is encoded by nucleotides 9784–9786. (b) Time course analysis of polypeptides synthesized in rabbit reticulocyte lysates from pIBV9Δ17 and pIBV9Q^{3086}–EΔ1. A 10-fold excess of unlabeled methionine was added to the *in vitro* translation reaction mixtures after incubation at 30°C for 10 min. Aliquots were subsequently taken from the reaction mixtures after incubation for 10, 20, 30, 40, 60, 90, and 120 min. The radiolabeled translation products were separated on an SDS–12.5% polyacrylamide gel and detected by fluorography.

and 49.66%, respectively, of the 3C-like proteinase. In a control experiment, the IBV membrane protein was exclusively detected in the membrane fraction (Fig. 6a, lane 6). Similarly, IBV-infected Vero cells were fractionated into the membrane and cytosol fractions. Immunoprecipitation and quantification assays showed that 76% of the 33-kDa proteinase was detected in the membrane fraction (Fig. 6b, lane 3), while only 24% of the protein was detected in the cytosol (Fig. 6b, lane 5). Once again, the IBV membrane protein was detected only in the membrane fraction (Fig. 6b, lane 4).

Identification of the Q^{3379}–A^{3380} dipeptide bond as a cleavage site of the 3C-like proteinase

The Q^{3365}–G^{3366} dipeptide bond encoded by nucleotides 10,621 to 10,626 was previously predicted to be a cleavage site of the 3C-like proteinase (Gorbalenya *et al.,* 1989). In a separate report, the Q^{3379}–A^{3380} dipeptide bond, which is located 14 amino acids downstream of the Q^{3365}–G^{3366} dipeptide bond and is conserved in all four sequenced coronaviruses (Lu *et al.,* 1998), was also predicted to be a cleavage site of the 3C-like proteinase (Lee *et al.,* 1991). The equivalent Q–A dipeptide bond of human coronavirus was actually identified as a genuine cleavage site (Ziebuhr and Siddell, 1999). In an *in vitro* study, Tibbles *et al.* (1999) recently reported that the Q^{3365}–G^{3366} dipeptide bond may be not used by the IBV 3C-like proteinase. However, the cleavability of the Q^{3379}–A^{3380} dipeptide bond was not mentioned in their report (Tibbles *et al.,* 1999). To further study whether either site is used by the IBV 3C-like proteinase, deletion and mutational analyses were carried out. As antiserum against this specific region was not available, the two downstream cleavage sites were disabled by site-directed mutagenesis, and anti-24 and antiserum V47 were used to immunoprecipitate the potential cleavage products (Ng and Liu, 1998) (Fig. 7a). Expression of pIBV1a16 resulted in the detection of the 33-kDa protein and a

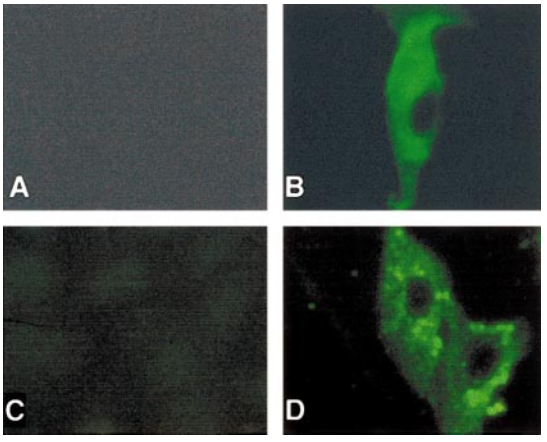

FIG. 5. Subcellular localization of the 3C-like proteinase. (A) Immunofluorescence staining of vTF7-infected Vero cells with anti-T7 monoclonal antibody (1:200). (B) Immunofluorescence staining of vTF7-infected and pIBVT7-3C-transfected Vero cells with anti-T7 monoclonal antibody (1:200) at 6 h posttransfection, showing cytoplasmic staining. (C) Immunofluorescence staining of the mock-infected Vero cells with anti-3C (1:20). (D) Immunofluorescence staining of IBV-infected Vero cells with anti-3C (1:20) at 13 h postinfection, showing distinct punctate perinuclear staining. All photos were taken with an epifluorescence microscope (Olympus Ix70, Tokyo), ×400.

protein of approximately 46 kDa (Fig. 7b, lanes 1 and 3). The 46-kDa protein may represent the C-terminal cleavage product with its N-terminus derived from cleavage at either the Q^{3365}–G^{3366} or Q^{3379}–A^{3380} dipeptide bond. Mutation of the Q^{3365} residue to an E did not change the expression pattern of the construct (Fig. 7b, lanes 2 and 4), indicating that the Q^{3365}–G^{3366} dipeptide bond may be not used. To confirm this possibility, the Q^{3365}–G^{3366} dipeptide bond was deleted from pIBV1a16, giving rise to pIBV1a16Δ1 (Fig. 7a). As can be seen in Fig. 7b, expression of pIBV1a16Δ1 resulted in the detection of both the 33- and the 46-kDa proteins and a product of approximately 52 kDa (lanes 5, 6, and 7). The 52-kDa protein may represent an intermediate cleavage product containing the 46-kDa protein and product encoded by the upstream region in this construct (Fig. 7a). As the 46-kDa cleavage product was still detected from this deletion construct, this result rules out the possibility that the Q^{3365}–G^{3366} dipeptide bond could be used by the 3C-like proteinase.

Similar deletion and mutational studies were then carried out to study whether the Q^{3379}–A^{3380} dipeptide bond is used by the proteinase to release the 46-kDa protein. Mutation of the Q^{3379} to an E led to the detection of only the 33- and 52-kDa products (Fig. 7b, lanes 8, 9, and 10). The 46-kDa protein was not detected (Fig. 7b, lanes 8 and 9), indicating that the Q^{3379} to E mutation blocks cleavage occurring at the Q^{3379}–A^{3380} dipeptide bond. This possibility was further studied by construction of pIBV1a16Δ2, which contains a deletion of nucleotides 9911 to 10,669 and thus excludes the Q^{3379}–A^{3380} dipeptide bond (Fig. 7a). Expression of this construct resulted in the detection of both the 33-kDa protein and a product migrating slightly more rapidly than the 52-kDa protein (Fig. 7b, lanes 11, 12, and 13). Its apparent molecular mass is approximately 51 kDa, which may represent the deleted version of the 52-kDa protein. Once again, the 46-kDa protein was not observed (Fig. 7b, lanes 11 and 12). These results confirmed that the Q^{3379}–A^{3380} dipeptide bond is a scissile bond of the 3C-like proteinase. Taken together with the previously identified Q^{3462}–S^{3463} dipeptide bond (Ng and Liu, 1998), cleavage at this position would result in the release of a mature product of approximately 9 kDa.

DISCUSSION

The IBV 3C-like proteinase plays a major role in processing of the gene 1-encoded polyproteins to smaller functional products associated with viral RNA replication. Previous studies using an *in vitro* processing assay showed that this proteinase may be released from the 1a polyprotein by self-cleavage at two Q–S dipeptide bonds

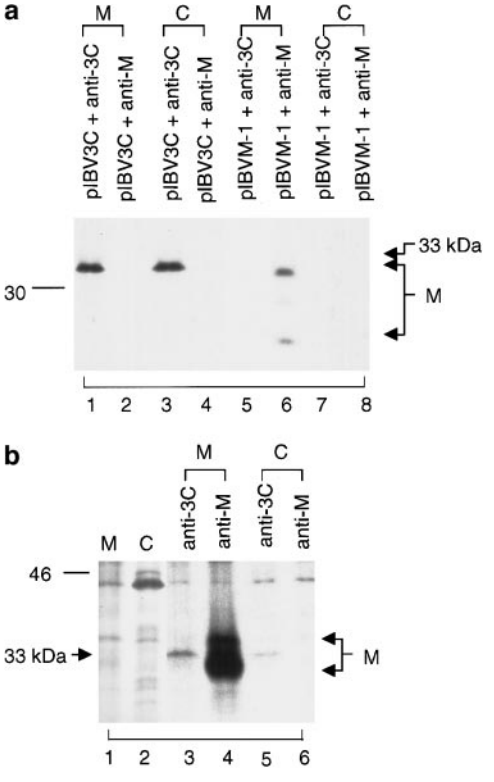

FIG. 6. (a) Subcellular fractionation of cells transiently expressing the 3C-like proteinase and IBV M protein, respectively. Cos-7 cells were transfected with appropriate plasmids and labeled with [^{35}S]methionine–cysteine. The cells were broken by a Dounce homogenizer and were fractionated into the membrane and cytosol fractions. Polypeptides in the two fractions were immunoprecipitated with anti-3C and anti-M, respectively. Gel electrophoresis of the polypeptides was performed on an SDS–12.5% polyacrylamide gel and polypeptides were detected by fluorography. (b) Subcellular fractionation of IBV-infected cells. Vero cells were infected with IBV, labeled with [^{35}S]methionine–cysteine, and fractionated into the membrane and cytosol fractions. Polypeptides were immunoprecipitated with anti-3C and anti-M.

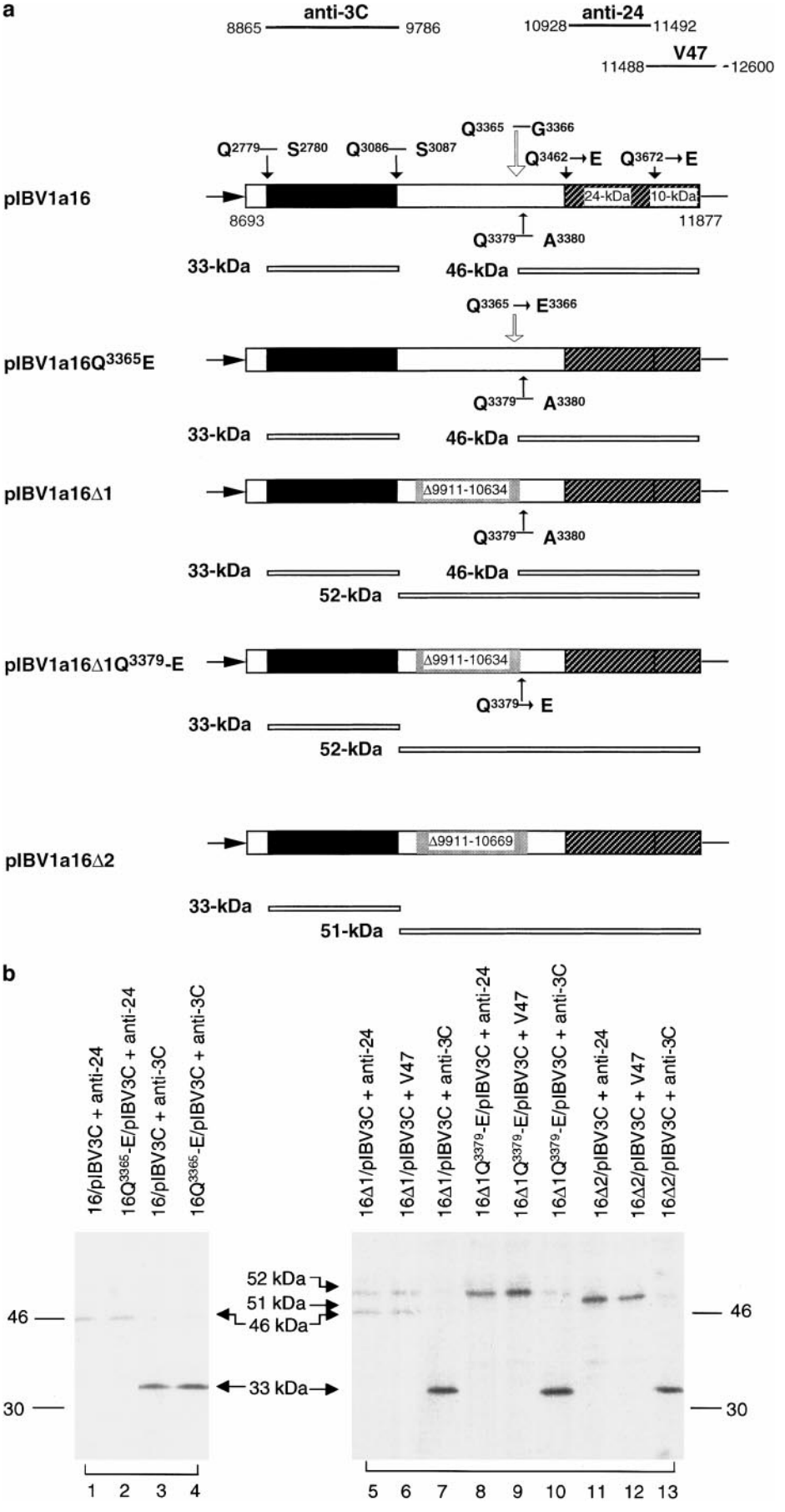
a
anti-3C
8865
9786
anti-24
10928
11492
V47
11488
12600
Q2779 S2780
Q3086 S3087
Q3365 G3366
Q3462 → E
Q3672 → E
pIBV1a16
24-kDa
10-kDa
8693
11877
Q3379 A3380
33-kDa
46-kDa
Q3365 → E3366
pIBV1a16Q3365E
pIBV1a16Δ1
Δ9911-10634
52-kDa
pIBV1a16Δ1Q3379-E
Q3379 → E
pIBV1a16Δ2
Δ9911-10669
51-kDa
b
16/pIBV3C + anti-24
16Q3365-E/pIBV3C + anti-24
16/pIBV3C + anti-3C
16Q3365-E/pIBV3C + anti-3C
16Δ1/pIBV3C + anti-24
16Δ1/pIBV3C + V47
16Δ1/pIBV3C + anti-3C
16Δ1Q3379-E/pIBV3C + anti-24
16Δ1Q3379-E/pIBV3C + V47
16Δ1Q3379-E/pIBV3C + anti-3C
16Δ2/pIBV3C + anti-24
16Δ2/pIBV3C + V47
16Δ2/pIBV3C + anti-3C
52 kDa
51 kDa
46 kDa
33 kDa
46
30
1 2 3 4 5 6 7 8 9 10 11 12 13

(Q^{2779}–S^{2780} and Q^{3086}–S^{3087}), and the *in vitro* enzymatic activity is strictly dependent on the addition of microsomal membranes (Tibbles *et al.,* 1996). In this study, we show that the IBV 3C-like proteinase is active *in vitro* even in the absence of microsomal membranes and that addition of the membranes only marginally increases the cleavage efficiency. Time-course and pulse–chase experiments further showed that efficient autoprocessing of the 3C-like proteinase occurs when the IBV sequence from nucleotide 8693 to 9911 was expressed *in vitro* (Fig. 4b). This is inconsistent with the results reported by Tibbles *et al.* (1996), showing no autoprocessing of the 3C-like proteinase when the same region was expressed *in vitro* even in the presence of microsomal membranes (Tibbles *et al.,* 1996). The reason for this discrepancy is currently unclear. However, the *in vitro* enzymatic activities of the IBV 3C-like proteinase reported here resemble the equivalent proteinase of human and murine coronaviruses. For example, the 3C-like proteinases of both human and murine coronaviruses are active when expressed *in vitro* (Heusipp *et al.,* 1997a; Lu *et al.,* 1995; Schiller *et al.,* 1998), and autoprocessing of the MHV 3C-like proteinase was slightly increased by the addition of microsomal membranes when only the upstream hydrophobic region was presented (Pinon *et al.,* 1997).

The mutagenesis studies presented here support the conclusion that the Q^{2779}–S^{2780} and Q^{3086}–S^{3087} dipeptide bonds are the N- and C-terminal cleavage sites, respectively, of the 3C-like proteinase. Interestingly, substantial cleavage was observed after mutation of either site to E–S, suggesting that the P1 position at these two sites are more tolerant to mutagenesis. However, much less tolerance to alterations at the P1 position was observed for the rest of the 11 cleavage sites identified so far (Liu *et al.,* 1997, 1998; Liu and Brown, 1995; Ng and Liu, 1998). The reasons for this difference are uncertain, but it may reflect the differing cleavage efficacy between the *cis*- and *trans*-enzymatic activities of the proteinase. The kinetic studies present here clearly indicate that cleavage first takes place at the Q^{2779}–S^{2780} dipeptide bond, which is followed by cleavage at the Q^{3086}–S^{30870} dipeptide bond, resulting in the release of the 3C-like proteinase. Cleavage at these two sites is therefore mediated by the *cis* activity of the proteinase. This process is very rapid and efficient, as no precursor containing the proteinase was detected even when the region was overexpressed in intact cells. Processing at other sites is thus likely mediated by the "free" 3C-like proteinase *in trans.* To argue against this speculation, Pinon *et al.* (1999) have recently reported that mutations of either the P1 or the P2 residue of the N-terminal QS site abolished *in vitro* autoprocessing of the MHV 3C-like proteinase.

Another interesting observation is that mutation of the Q^{3086} residue to an E alters the mobility of the 33-kDa proteinase on SDS–PAGE, yet almost full enzymatic activity of the proteinase is maintained. Mutation of the equivalent Q^{3267} residue of HCV-229E 3C-like proteinase to an A exerts no effect on the proteinase activity, although information on the mobility of this mutant on SDS–PAGE was not available (Ziebuhr *et al.,* 1997). Deletion of up to 7 amino acids from the C-terminus of the IBV 3C-like proteinase renders no significant effect on the enzymatic activity of the proteinase. Progressive loss of the activity was observed when further deletions were made. Interestingly, significant enzymatic activity was still maintained when the C-terminal 67 amino acid residues were deleted. Furthermore, the three mutant forms (the Q^{3086}–E mutant and the two mutants with deletions of 3 and 7 amino acids) migrate on SDS–PAGE significantly more slowly than the wild-type proteinase. These results suggest that the extreme C-terminal region may be able to fold into a unique structure independent of the catalytic domain, which is located at the N-terminal half of the protein. Cotranslational folding of a functionally active proteinase domain may occur even before the whole proteinase is synthesized. This argument would be supported by several recent studies on eukaryotic protein folding. It was demonstrated that rapid and efficient folding of modular model proteins depends on sequential folding of their domains during synthesis (Netzer and Hartl, 1997; Nicola *et al.,* 1999; Louis *et al.,* 1999). Cotranslational folding of two proteinase domains with enzymatic activities was observed when the novel polypeptide chains were still bound to the ribosome (Nicola *et al.,* 1999; Louis *et al.,* 1999). This is in contrast to the protein folding in prokaryotic system, in which the folding of a functional domain occurs posttranslationally (Netzer and Hartl, 1997). This different folding mechanism may explain the data reported by Ziebuhr *et al.* (1997), showing that the HCV-229E 3C-like proteinase expressed in bacteria was inactivated by deletion of the C-terminal 33 amino acid residues.

Immunofluorescence staining of coronavirus-infected cells using anti-3C antibodies reveals distinct perinuclear, puctate staining patterns in several recent reports (van der Meer *et al.,* 1998, 1999; Schiller *et al.,* 1998; Shi

FIG. 7. (a) Diagram of pIBV1a16, pIBV1a16Q^{3365}–E, pIBV1a16Δ1, pIBV1a16Δ1Q^{3379}–E, and pIBV1a16Δ2, showing the locations of the cleavage sites and the substitution mutations that were introduced. The viral products generated from cleavage by the 3C-like proteinase are illustrated, and the molecular masses of these products were estimated according to their migration on SDS–PAGE. The Q^{2779}–S^{2780}, Q^{3086}–S^{3087}, Q^{3365}–G^{3366}, Q^{3379}–A^{3380}, Q^{3462}, and Q^{3672} residues are encoded by nucleotides 8863–8868, 9784–9789, 10,621–10,626, 10,663–10,668, 10,912–10,914 and 11,542–11,544, respectively. (b) Mutation and deletion analyses of the Q^{3379}–A^{3380} dipeptide bond. Plasmids pIBV1a16Δ1, pIBV1a16Δ1Q^{3379}–E, and pIBV1a16Δ2 were expressed in Cos-7 cells using the vaccinia-T7 system. Cells were labeled with [^{35}S]methionine–cysteine and total lysates were immunoprecipitated with anti-24 and anti-3C, respectively. Polypeptides were separated on an SDS–12.5% polyacrylamide gel and detected by fluorography.

et al., 1999). As rapid self-cleavage of the 3C-like proteinase from the polyprotein precursors was reported for these viruses, these staining patterns should be contributed mainly by the staining of the mature 3C-like proteinase. In this report, we present evidence showing that the IBV 3C-like protein displays a free distribution pattern when it was expressed in intact cells alone. However, in IBV-infected cells, the proteinase is associated mainly with the intracellular membranes. Two possibilities may be responsible for these different distribution patterns. First, the 3C-like proteinase may be sequestered to cellular membranous compartments by interacting with other viral or cellular proteins. Recently, we showed that anti-3C antiserum could immunoprecipitate a protein band of about 170 kDa in IBV-infected cells (Lim *et al.,* 2000). The same protein species could also be detected by several other IBV region-specific antisera (Lim *et al.,* 2000). As the 170-kDa protein may be an IBV-induced host protein, it is tempting to speculate that the IBV 3C like proteinase together with other viral products may interact with this protein to form a multiprotein complex involved in viral replication. The second possibility is that the IBV 3C-like proteinase may be able to bind to viral RNA. In poliovirus, the viral 3C proteinase was shown to be an RNA binding protein (Andino *et al.,* 1993). The 3C proteinase and polymerase precursor (3CD) together with a cellular protein can form a ribonucleoprotein complex with the first 90 nucleotides of the poliovirus genome (Andino *et al.,* 1993). This complex may play an important role in the replication of polioviral RNA. We are currently unclear whether the IBV 3C-like proteinase may be involved in the formation of coronavirus replication complexes.

MATERIALS AND METHODS

Virus and cells

The egg-adapted Beaudette strain of IBV (ATCC VR-22) was obtained from the American Type Culture Collection (ATCC) and was adapted to Vero cells as described previously (Ng and Liu, 1998). The virus was passaged three times in 11-day-old chicken embryos and then adapted to Vero cells (ATCC CCL-81) by a series of passages at 24- to 48-h intervals. The cytopathic effects, including syncytium formation and rounding-up of cells, were initially observed after three passages in Vero cells. Virus stocks were prepared after the 62nd passage by infecting monolayers of Vero cells at a multiplicity of infection of approximately 0.1 PFU/cell. The virus was harvested at 24 h postinfection and the titer of the virus preparation was determined by plaque assay on Vero cells.

Vero cells and Cos-7 cells were grown at 37°C in 5% CO_2 and maintained in Dulbecco's modified minimal essential medium (Gibco BRL, Life Technologies) supplemented with 10% newborn calf serum.

Radiolabeling of IBV-infected and mock-infected Vero cells

Confluent monolayers of Vero cells grown on 60-mm dishes were infected with IBV at a multiplicity of infection of approximately 2 PFU/cell. The cells were labeled for 4 h with 25 μCi/ml [^{35}S]methionine–cysteine at 6 h postinfection before harvesting.

Transient expression of plasmid DNAs using the vaccinia virus-T7 expression system

Semiconfluent monolayers of Cos-7 cells grown on 60-mm dishes were infected with 10 PFU/cell of vTF7-3 (Fuerst *et al.,* 1986) and transfected with 2.5 μg of plasmid DNAs using 15 μl of DOTAP liposomal transfection reagent according to the instructions of the manufacturer (Boehringer Mannheim). After incubation of the cells at 37°C for 7 h, the cells were incubated in methionine- and cysteine-free medium (ICN) for 30 min and labeled with 25 μCi/ml [^{35}S]methionine–cysteine (35S Express Protein Labelling Mix, NEN Life Science) for 13 h. The cells were scraped off the dishes in phosphate-buffered saline (PBS) and recovered by centrifugation at 12,000 rpm for 1 min.

Cell fractionation of [^{35}S]methionine–cysteine-labeled cells

The radiolabeled cells were resuspended in hypotonic buffer (1 mM Tris–HCl, pH 7.4, 0.1 mM EDTA, 15 mM NaCl) containing 2 μg/ml leupeptin and 0.4 mM phenylmethylsulfonyl fluoride (PMSF) and broken by 20 strokes with a Dounce cell homogenizer as described (van der Meer *et al.,* 1998). Cell debris and nuclei were removed by centrifugation at 3500 rpm for 10 min at 4°C. The membranes were pelleted by ultracentrifugation in a Beckman TLA 120.1 rotor (65,000 rpm for 30 min at 4°C). Membrane pellets were resuspended in immunoprecipitation buffer [20 mM Tris–HCl, pH 7.4, 5 mM EDTA, 150 mM NaCl, 0.5% SDS, 0.1% sodium deoxycholate, 0.5% Nonidet-P40 (NP-40)] and the cytosol fraction (supernatant) was adjusted to the same volume and ion/detergent conditions with 2× immunoprecipitation buffer. Samples were precleared by centrifugation and incubated with anti-3C or anti-M for 30 min at room temperature, followed by 30 min incubation with protein A–Sepharose CL-4B (Sigma). Immunoprecipitated beads were washed three times with the immunoprecipitation buffer and analyzed by SDS–PAGE.

SDS–polyacrylamide gel electrophoresis

SDS–PAGE was carried out with a 12.5% polyacrylamide concentration, and the labeled polypeptides were detected by autoradiography or fluorography of dried gels.

Cell-free transcription and translation

Plasmid DNAs were expressed in rabbit reticulocyte lysate using a transcription coupled translation system (TnT, Promega) in the presence of [^{35}S]methionine (Amersham-Pharmacia Biotech) according to the instructions of the manufacturer. Briefly, 1 μg of plasmid DNA was incubated in a 50-μl reaction mix with or without 5 μl of canine pancreatic microsomal membranes (Promega). Aliquots were either analyzed directly by SDS–PAGE or immunoprecipitated with polyclonal antiserum as described previously (Liu *et al.,* 1997).

Polymerase chain reaction (PCR)

Appropriate primers and template DNAs were used in amplification reactions with cloned *Pfu* DNA polymerase (Stratagene) under standard buffer conditions with 2 mM $MgCl_2$.

Indirect immunofluorescence microscopy

Cells were grown on coverslips and infected with IBV or transfected with appropriate plasmid DNAs. After being washed with PBS containing 1 mM $CaCl_2$ and 1 mM $MgCl_2$ (PBSCM), the cells were fixed with 4% paraformaldehyde (in PBSCM) for 30 min at room temperature and permeabilized with 0.1% saponin (in PBSCM), followed by incubation with specific antiserum (anti-3C) at room temperature for 2 h. Antibodies were diluted in fluorescence dilution buffer (PBSCM with 5% normal goat serum, 5% newborn calf serum, and 2% bovine serum albumin, pH 7.6). The cells were then washed with PBSCM and incubated with anti-rabbit IgG conjugated to fluorescein isothiocynate (1:80, Sigma) in the fluorescence dilution buffer at 4°C for 1 h before being mounted.

Site-directed mutagenesis

Site-directed mutagenesis was carried out by two rounds of PCR with two pairs of primers as described (Liu *et al.,* 1997). The mutations introduced were verified by automated nucleotide sequencing.

Construction of plasmids

Plasmids pIBV9 (formerly known as pKT205), pIBV3C, pBP5Δ5, and pIBV1a7Δ1 were described previously (Liu *et al.,* 1994, 1997; Lim *et al.,* 2000). The IBV sequences present in these constructs are nucleotides 8693 to 10,925, 8865 to 9786, 11,306 to 11,877, 6870 to 9786, and 7999 to 9786, respectively.

Plasmid pIBV9Δ1Q^{2779}–E, which contains the Q^{2779}–E mutation and a deletion of nucleotides 9911 to 10,925 from pIBV9, was constructed as follows. A PCR fragment covering nucleotides 8693 to 10,637 was generated by two rounds of PCR with pIBV9 as the template. The PCR fragment was digested with *Bgl*II and *Pvu*II and cloned into *Bgl*II- and *Sma*I-digested pKT0 (Liu *et al.,* 1994) (see Fig. 2a). *Pvu*II cuts the IBV sequence at nucleotide position 9911 and *Bgl*II digests the PCR fragment at a position 19 nucleotides upstream of the viral sequence. The primers used to introduce the Q^{2779}–E mutation are LN-10 (5′-GTTAGTAGATTAGAGTCTGGTTTTAAG-3′) and LN-11 (5′-CAGTTTCTTAAAACCAGACTCTAATCT-3′), and the primers used for the second round of PCR are T7 (5′-TAATACGACTCACTATAGGG-3′) and LN-8 (5′-GTCACCACCAATTCCCTCTATAAGTAT-3′). Plasmid pIBV9Δ1Q^{2779}–K was generated as described for pIBV9Δ1Q^{2779}–E by mutation of the Q^{2779} residue to a K with primers LN-32 (5′-GTTAGTAGATTAAAGTCTGGTTTTAAG-3′) and LN-33 (5′-CAGTTTCTTAAAACCAGACTTTAATCTAC-3′).

Plasmid pIBV9Q^{3086}–E contains the Q^{3086}–E mutation and a deletion of nucleotides 10,637 to 10,925 from pIBV9. The mutation and deletion were introduced by two rounds of PCR with pIBV9 as the template. The PCR fragment was digested with *Bgl*II and cloned into *Bgl*II- and *Eco*RV-digested pKT0, giving rise to pIBV9Q^{3086}–E. The mutation primers are LN-12 (5′-GGTGTTAGATTAGAGTCTTCTTTTGTA-3′) and LN-13 (5′-AGCTTTTCTTACAAAAGAAGACTCTAATCT-3′), and the two primers used for the second round of PCR are T7 and LN-8. Plasmid pIBV9Q^{3086}–EΔ1, which covers nucleotides 8693 to 9910 and contains the Q^{3086}–E mutation, was constructed by religation of *Pvu*II- and *Sma*I-digested pIBV9Q^{3086}–E, resulting in the deletion of nucleotides 9911 to 10,637. Plasmid pIBV9Q^{3086}–EΔ2 was constructed by introducing a termination codon (UAG) immediately downstream of the codon coding for the E^{3086} residue. The primer used to introduce this mutation is LN-29 (5′-AGAAGAGAGCTCTACTCTAATCTAACAC-3′).

Plasmid pIBV9Δ17, which covers nucleotides 8693 to 9910, was constructed by religation of *Pvu*II- and *Sma*I-digested pIBV9, resulting in the deletion of nucleotides 9911 to 10,925.

Plasmids pIBV9Δ19, pIBV9Δ20, pIBV9Δ21, pIBV9Δ22, and pIBV9Δ23 cover nucleotides 8693 to 9777, 8693 to 9765, 8693 to 9687, 8693 to 9585, and 8693 to 9381, respectively, and contain a UAG termination codon immediately downstream of the viral sequences. The constructs were made by ligation of PCR fragments covering the appropriate regions into pKT0. The PCR fragments were generated using pIBV9 as the template and T7 as the upstream primer. The downstream primers are LN61 (5′-TAATCTGAGCTCTAAACACCACCAATCTG-3′), LN62 (5′-ACCAATGAGCTCTACTGATTAAATACAGA-3′), LN63 (5′-CTGGCTGAGCTCTAATTTTTTACCATAAT-3′), LN64 (5′-ACCATTGAGCTCTAGTCACCAGCCCACTT-3′), and LN65 (5′-GTCAGTGAGCTCTATCCAGTGTGTAATGC-3′), respectively.

Plasmid pIBV1a16 covers nucleotides 8693 to 11,877 and contains both Q^{3462}–E and Q^{3672}–E mutations. The two mutations were introduced into a PCR fragment covering nucleotides 8693 to 11,877 as follows. The Q^{3672}–E mutation was incorporated into the PCR fragment

by using pBP5Δ5Q^{3672}–E (Liu *et al.,* 1997) as the template, and the Q^{3462}–E mutation was introduced by primers X-38 (5′-CAACTGTATTAGAATCGGTTAC-3′) and LN-2 (5′-CTTGAGTAACCGATTCTAATACAGTTG-3′). This PCR fragment was cloned into pKT0, giving rise to pIBV1a16. Plasmid pIBV1a16Q^{3365}–E, which contains the Q^{3365}–E mutation (see Fig. 8a), was constructed by two rounds of PCR with pIBV1a16 as the template. The primers used to introduce the Q^{3365}–E mutation were LN-7 (5′-TCGACAAATATACTTATAGAGGGAATTGG-3′) and LN-8.

Plasmid pIBV1a16Δ1 covers nucleotides 8693 to 11,877 with a deletion of nucleotides 9911 to 10,634. It was made by digestion of pIBV1a16 with *Bst*EII (which cuts at nucleotide 10,634), end-repair with Klenow, redigestion with *Pvu*II (cuts at nucleotide 9911), and religation with T4 DNA ligase, resulting in the deletion of nucleotides 9911 to 10,634. pIBV1a16Δ2 was constructed by deletion of nucleotides 9911 to 10,669 from pIBV1a16.

Plasmid pIBV1a16Δ1Q^{3379}–E, which covers nucleotides 8693 to 11,877 with the Q^{3379} to E mutation, was made by two rounds of PCR with pIBV1a16Δ1 as the template. The primers used to introduce the Q^{3379} to E mutation are LN-22 (5′-CTATTGCTACAGTTGAGGCTAAATTGAGT-3′) and LN-23 (5′-TACATCACTCAATTTAGCCTCAACTGTAG-3′), and the cloning primers are T7 and LDX-7 (5′-GCTCCAGGATCCTACTGTAAGACAAC-3′).

ACKNOWLEDGMENTS

We thank Ms. Haoying Xu for excellent technical assistance. This work was supported by a grant from the National Science and Technology Board of Singapore.

REFERENCES

Andino, R., Rieckhof, G. E., Achacoso, P. L., and Baltimore, D. (1993). Poliovirus RNA synthesis utilizes an RNP complex formed around the 5′-end of viral RNA. *EMBO J.* **12,** 3587–3598.

Baker, S. C., Shieh, C.-K., Soe, L. H., Chang, M.-F., Vannier, D. M., and Lai, M. M. C. (1989). Identification of a domain required for autoproteolytic cleavage of murine coronavirus gene A polyprotein. *J. Virol.* **64,** 3693–3699.

Baker, S. C., Yokomori, K., Dong, S., Carlise, R., Gorbalenya, A. E., Koonin, E. V., and Lai, M. M. C. (1993). Identification of the catalytic sites of a papain-like cysteine proteinase of murine coronavirus. *J. Virol.* **67,** 6056–6063.

Bonilla, P. J., Hughes, S. A., and Weiss, S. R. (1997). Characterization of a second cleavage site and demonstration of activity *in trans* by the papain-like proteinase of the murine coronavirus mouse hepatitis virus strain A59. *J. Virol.* **71,** 900–909.

Boursnell, M. E. G., Brown, T. D. K., Foulds, I. J., Green, P. F., Tomely, F. M., and Binns, M. M. (1987). Completion of the sequence of the genome of the coronavirus avian infectious bronchitis virus. *J. Gen. Virol.* **68,** 57–77.

Brierley, I., Boursnell, M. E. G., Binns, M. M., Bilimoria, B., Blok, V. C., Brown, T. D. K., and Inglis, S. C. (1987). An efficient ribosomal frame-shifting signal in the polymerase-encoding region of the coronavirus IBV. *EMBO J.* **6,** 3779–3785.

Brierley, I., Digard, P., and Inglis, S. C. (1989). Characterization of an efficient coronavirus ribosomal frameshifting signal: Requirement for an RNA pseudoknot. *Cell* **57,** 537–547.

Cavanagh, D. (1997). Nidovirales: A new order comprising *Coronaviridae* and *Arteriviridae. Arch. Virol.* **14,** 629–633.

Denison, M. R., Spaan, W. J. M., van der Meer, Y., Gibson, C. A., Sims, A. C., Prentice, E., and Lu, X. T. (1999). The putative helicase of the coronavirus mouse hepatitis virus is processed from the replicase gene polyprotein and localizes in complexes that are active in viral RNA synthesis. *J. Virol.* **73,** 6862–6871.

de Vries, A. A. F., Horzinek, M. C., Rottier, P. J. M., and de Groot, R. J. (1997). The genome organization of the *Nidovirales:* Similarities and differences between arteri-, toro-, and coronaviruses. *Semin. Virol.* **8,** 33–47.

Dong, S. H., and Baker, S. C. (1994). Determination of the p28 cleavage site recognized by the first papain-like cysteine proteinase of murine coronavirus. *Virology* **204,** 541–549.

Fuerst, T. R., Niles, E. G., Studier, F. W., and Moss, B. (1986). Eukaryotic transient-expression system based on recombinant vaccinia virus that synthesizes bacteriophage T7 RNA polymerase. *Proc. Natl. Acad. Sci. USA* **83,** 8122–8127.

Gao, H. Q., Schiller, J. J., and Baker, S. C. (1996). Identification of the polymerase polyprotein products p72 and p65 of the murine coronavirus MHV-JHM. *Virus Res.* **45,** 101–109.

Gorbalenya, A. E., Koonin, E. V., Donchenko, A. P., and Blinov, V. M. (1989). Coronavirus genome: Prediction of putative functional domains in the non-structural polyprotein by comparative amino acid sequence analysis. *Nucleic Acids Res.* **17,** 4847–4861.

Grotzinger, C., Heusipp, G., Ziebuhr, J., Harms, U., Suss, J., and Siddell, S. G. (1996). Characterization of a 105-kDa polypeptide encoded in gene 1 of the human coronavirus HCV 229E. *Virology* **222,** 227–235.

Herold, J., Gorbalenya, A. E., Thiel, V., Schelle, B., and Siddell, S. G. (1998). Proteolytic processing at the amino terminus of human coronavirus 229E gene 1-encoded polyproteins: Identification of a papain-like proteinase and its substrate. *J. Virol.* **72,** 910–918.

Heusipp, G., Grotzinger, C., Herold, J., Siddell, S. G., and Ziebuhr, J. (1997a). Identification and subcellular localization of a 41 kDa, polyprotein 1ab processing product in human coronavirus 229E-infected cells. *J. Gen. Virol.* **78,** 2789–2794.

Heusipp, G., Harms, U., Siddell, S. G., and Ziebuhr, J. (1997b). Identification of an ATPase activity associated with a 71-kilodalton polypeptide encoded in gene 1 of the human coronavirus 229E. *J. Virol.* **71,** 5631–5634.

Hughes, S. A., Bonilla, P. J., and Weiss, S. R. (1995). Identification of the murine coronavirus p28 cleavage site. *J. Virol.* **69,** 809–813.

Lee, H. J., Shieh, C.-K., Gorbalenya, A. E., Koonin, E. V., la Monica, N., Tuler, J., Bagdzhadzhyan, A., and Lai, M. M. C. (1991). The complete sequence (22 kilobases) of murine coronavirus gene 1 encoding the putative proteases and RNA polymerase. *Virology* **180,** 567–582.

Lim, K. P., and Liu, D. X. (1998). Characterization of the two overlapping papain-like proteinase domains encoded in gene 1 of the coronavirus infectious bronchitis virus and determination of the C-terminal cleavage site of an 87-kDa protein. *Virology* **245,** 303–312.

Lim, K. P., Ng, L. F. P., and Liu, D. X. (2000). Identification of a novel cleavage activity of the first papain-like proteinase domain encoded by ORF 1a of the coronavirus avian infectious bronchitis virus and characterization of the cleavage products. *J. Virol.* **74,** in press.

Liu, D. X., Brierley, I., Tibbles, K. W., and Brown, T. D. K. (1994). A 100-kilodalton polypeptide encoded by open reading frame (ORF) 1b of the coronavirus infectious bronchitis virus is processed by ORF 1a products. *J. Virol.* **68,** 5772–5780.

Liu, D. X., Tibbles, K. W., Cavanagh, D., Brown, T. D. K., and Brierley, I. (1995). Identification, expression, and processing of an 87 kDa polypeptide encoded by ORF 1a of the coronavirus infectious bronchitis virus. *Virology* **208,** 48–57.

Liu, D. X., and Brown, T. D. K. (1995). Characterization and mutational analysis of an ORF-1a-encoding proteinase domain responsible for proteolytic processing of the infectious bronchitis virus 1a/1b polyprotein. *Virology* **209,** 420–427.

Liu, D. X., Xu, H. Y., and Brown, T. D. K. (1997). Proteolytic processing of the coronavirus infectious bronchitis virus 1a polyprotein: Identifica-

tion of a 10-kilodalton polypeptide and determination of its cleavage sites. *J. Virol.* **71,** 1814–1820.

Liu, D. X., Shen, S., Xu, H. Y., and Wang, S. F. (1998). Proteolytic mapping of the coronavirus infectious bronchitis virus 1b polyprotein: Evidence for the presence of four cleavage sites of the 3C-like proteinase and identification of two novel cleavage products. *Virology* **246,** 288–297.

Louis, J. M., Clore, G. M., and Gronenborn, A. M. (1999). Autoprocessing of HIV-1 protease is tightly coupled to protein folding. *Nat. Struct. Biol.* **6,** 868–875.

Lu, X. T., Lu, Y., and Denison, M. R. (1996). Intracellular and *in vitro* translated 27-kDa proteins contain the 3C-like proteinase activity of the coronavirus MHV-A59. *Virology* **222,** 375–382.

Lu, X. T., Sims, A. C., and Denison, M. R. (1998). Mouse hepatitis virus 3C-like protease cleaves a 22-kilodalton protein from the open-reading frame 1a polyprotein in virus-infected cells and *in vitro*. *J. Virol.* **72,** 2265–2271.

Lu, Y., Lu, X. T., and Denison, M. R. (1995). Identification and characterization of a serine-like proteinase of the murine coronavirus MHV-A59. *J. Virol.* **69,** 3554–3559.

Netzer, W., and Hartl, F. U. (1997). Recombination of protein domains facilitated by co-translational folding in eukaryotes. *Nature* **388,** 343–349.

Ng, L. F. P., and Liu, D. X. (1998). Identification of a 24-kDa polypeptide processed from the coronavirus infectious bronchitis virus 1a polyprotein by the 3C-like proteinase and determination of its cleavage sites. *Virology* **243,** 388–395.

Nicola, A. V., Chen, W., and Helenius, A. (1999). Co-translational folding of an alphavirus capsid protein in the cytosol of living cells. *Nat. Cell Biol.* **1,** 341–345.

Pinon, J. D., Mayreddy, R. R., Turner, J. D., Khan, F. S., Bonilla, P. J., and Weiss, S. R. (1997). Efficient autoproteolytic processing of the MHV-A59 3C-like proteinase from the flanking hydrophobic domains requires membranes. *Virology* **230,** 309–322.

Pinon, J. D., Teng, H., and Weiss, S. R. (1999). Further requirements for cleavage by the murine coronavirus 3C-like proteinase: Identification of a cleavage site within ORF1b. *Virology* **263,** 471–484.

Schiller, J. J., Kanjanahaluethai, A., and Baker, S. C. (1998). Processing of the coronavirus MHV-JHM polymerase polyprotein: Identification of precursors and proteolytic products spanning 400 kilodaltons of ORF1a. *Virology* **242,** 288–302.

Seybert, A., Ziebuhr, J., and Siddell, S. G. (1997). Expression and characterization of a recombinant murine coronavirus 3C-like proteinase. *J. Gen. Virol.* **78,** 71–75.

Shi, S. T., Schiller, J. J., Kanjanahaluethai, A., Baker, S. C., Oh, J.-W., and Lai, M. M. C. (1999). Colocalization and membrane association of murine hepatitis virus gene 1 products and de novo-synthesized viral RNA in infected cells. *J. Virol.* **73,** 5957–5969.

Tibbles, K. W., Brierley, I., Cavanagh, D., and Brown, T. D. K. (1996). Characterization *in vitro* of an autocatalytic processing activity associated with the predicted 3C-like proteinase domain of the coronavirus avian infectious bronchitis virus. *J. Virol.* **70,** 1923–1930.

Tibbles, K. W., Cavanagh, D., and Brown, T. D. K. (1999). Activity of a purified His-tagged 3C-like proteinase from the coronavirus infectious bronchitis virus. *Virus Res.* **60,** 137–145.

van der Meer, Y., van Tol, H., Locker, J. K., and Snijder, E. J. (1998). ORF1a-encoded replicase subunits are involved in the membrane association of the arterivirus replication complex. *J. Virol.* **72,** 6689–6698.

van der Meer, Y., Snijder, E. J., Dobbe, J. C., Schleich, S., Denison, M. R., Spaan, W. J. M., and Locker, J. K. (1999). Localization of mouse hepatitis virus nonstructural proteins and RNA synthesis indicates a role for late endosomes in viral replication. *J. Virol.* **73,** 7641–7657.

Ziebuhr, J., Herold, J., and Siddell, S. G. (1995). Characterization of a human coronavirus (strain 229E) 3C-like proteinase activity. *J. Virol.* **69,** 4331–4338.

Ziebuhr, J., Heusipp, G., and Siddell, S. G. (1997). Biosynthesis, purification, and characterization of the human coronavirus 229E 3C-like proteinase. *J. Virol.* **71,** 3992–3997.

Ziebuhr, J., and Siddell, S. G. (1999). Processing of the human coronavirus 229E replicase polyproteins by the virus-encoded 3C-like proteinase: Identification of proteolytic products and cleavage sites common to pp1a and pp1ab. *J. Virol.* **73,** 177–185.